Applied Clay Science 83–84 (2013) 280–285

Contents lists available at ScienceDirect

Applied Clay Science

journal homepage: www.elsevier.com/locate/clay

Research paper

ODTMA$^+$ and HDTMA$^+$ organo-montmorillonites characterization: New insight by WAXS, SAXS and surface charge

A.E. Bianchi [a,b], M. Fernández [b,c], M. Pantanetti [c], R. Viña [a], I. Torriani [d], R.M. Torres Sánchez [c,*], G. Punte [a,**]

[a] LANADI-IFLP (CCT-La Plata), Departamento de Física, Facultad de Ciencias Exactas, Universidad Nacional de La Plata CC67, 1900 La Plata, Argentina
[b] Facultad de Ingeniería, Departamento de Ciencias Básicas, Universidad Nacional de La Plata, 115 y 49, 1900 La Plata, Argentina
[c] CETMIC-CCT La Plata, Camino Centenario y 506, (1897) M. B. Gonnet, La Plata, Argentina
[d] DFMC-UNICAMP and LNLS, Campinas, SP, Brazil

ARTICLE INFO

Article history:
Received 14 December 2011
Received in revised form 12 August 2013
Accepted 13 August 2013
Available online 14 September 2013

Keywords:
Montmorillonite
Organo-montmorillonite
SAXS
Zeta potential

ABSTRACT

In this work we investigate the microstructure and properties of organo-montmorillonites (OMts) synthesized by intercalation of a Patagonian Mt with different surfactant/CEC ratios (0.5, 1 and 2) of octadecyl trimethylammonium (ODTMA$^+$) and hexadecyl trimethylammonium (HDTMA$^+$) cations. X-ray diffraction (XRD) patterns showed that in all OMt samples d_{001} value increases with respect to raw Mt (1.258 nm). Small angle and wide angle X-ray scattering (SAXS and WAXS) curves, particle apparent diameters (determined by laser), zeta potential values and scanning electron microscopy (SEM) images, showed the presence of assorted d_{001} values (which depend on storage conditions), aggregate formation and charge reversal (which varied with loading and cation length) for samples obtained with 1 and 2 CEC. However, for samples intercalated with 0.5 CEC, we found evidence of smaller aggregate formation, no charge reversal, and similar d_{001} and zeta potential values (both higher than those of Mt). Findings reported here will help attain better conditions to functionalize highly charged Mt making them suitable to be used as nanocomposite precursors for different applications.

1. Introduction

Clay minerals, as montmorillonite (Mt), had been of interest for the development or improvement of materials for various applications due to their availability, and low cost and the possibility of changing their physicochemical properties by different methods. Since the 1940s the exchange of the Mt interlayer metal cations with organic surfactant cations (commonly alkylammonium cations) has been extensively studied (Alexandre and Dubois, 2000; He et al., 2010; Lagaly, 1986, 1994; Lagaly et al., 1984; Lin et al., 2003; Williams-Daryn and Thomas, 2002; Zhao et al., 2003; Zhu et al., 2011). Recently, incorporation of neutral amines (Li and Ishida, 2003) and cations with polar groups (Tiwari et al., 2008) has also proved to render swollen and ordered organo-clay minerals.

Among the different applications found for the organo-montmorillonites (OMts), the improvement of polymer properties has been one of the most important — for a recent review see De Paiva et al. (2008). Kojima et al. (1993) and Botana et al. (2010) (and references cited therein) have shown that the incorporation of small quantities of these OMt (5-10% in mass) allows changing the stiffness and toughness of the final polymers, expands their barrier properties, their resistance to fire and ignition, etc.

The formation of barrier-layers has been widely argued as the theoretical support for the enhanced burning behavior of clay polymer nanocomposites (CPNs) (Isitman and Kaynak, 2011). However, other studies (Fox et al., 2010) question the suggested mechanism.

Some authors have proposed that the upgrading of polymer properties is highly dependent on the degree of smectite dispersion (Kornmann et al., 2001), while others observed that the smectite orientation and aspect ratio influence CPN mechanical properties and the heat distortion temperature (Weon and Sue, 2005). Vaia and Wagner (2004) and Benetti et al. (2005) remarked the importance of a large interfacial area per volume of particles for CPNs' use as components of active devices. Accordingly, the performance of CPNs will depend strongly on the breaking-up of smectite particles in the polymer matrix and, therefore, an exfoliated smectite structure within the matrix will be the most suitable for technological applications since it maximizes the interfacial area.

The above considerations indicate that appropriate organo-montmorillonites would be those with low exfoliation energy. Pospíšil et al. (2002, 2004) studied the influence of intercalation of different surfactants and surfactant contents on the exfoliation energy of montmorillonites.

Several techniques have been applied to investigate the nature of the above mentioned complex mechanism. The surfactant intercalation and arrangement in the interlayer space of Mt have been followed by XRD

* Corresponding author. Tel.: +54 221 484 0247/0167x119; fax: +54 221 471 0075.
** Corresponding author. Tel.: +54 221 424 6062/7201x258/287; fax: +54 221 425 2006.
E-mail addresses: rosats@cetmic.unlp.edu.ar (R.M.T. Sánchez), punte@fisica.unlp.edu.ar (G. Punte).

0169-1317/$ – see front matter © 2013 Elsevier B.V. All rights reserved.
http://dx.doi.org/10.1016/j.clay.2013.08.032

through Mt swelling determination (Hendricks and Teller, 1942). SEM data were utilized to examine changes in the obtained OMt samples' morphology (He et al., 2006). Comparison of zeta potential values of attained products with raw Mt could reveal adsorption of surfactants on the external surface (Thomas et al., 1999). Many contradictory results can be found in the literature regarding cation substitution degree and OMt sample homogeneity. They seemed to be related to small differences in the synthesis process, aging, storage conditions and smectite surface charge density or distribution (De Paiva et al., 2008; Lee et al., 2005; Zhu et al., 2011).

In this work some properties of a raw Patagonian Mt and two OMts produced by cation substitution for octadecyl trimethylammonium ($ODTMA^+$) and hexadecyl trimethylammonium ($HDTMA^+$) in different proportions in the raw Mt are explored.

The samples were characterized by a specific surface area, apparent particle diameter (D_{app}), XRD, SEM and zeta potential determinations. To get information not available to standard X-ray diffractometers, SAXS and WAXS experiments employing a synchrotron light source have also been performed.

2. Experimental

2.1. Materials

Patagonian montmorillonite, provided by Castiglioni Pes y Cia., was used as received and named Mt. The main properties of this Mt, determined in a previous work (Magnoli et al., 2008), are: cation exchange capacity (CEC) 174 meq/100 g, isoelectric point (IEP) at pH = 2.7, external specific surface area (determined by N_2 adsorption) 34.0 m^2/g and total specific surface area (determined by water vapor adsorption, Michot and Villieras, 2006) 621 m^2/g. The sample contained 84, 12 and 4% of montmorillonite, quartz and feldspar, respectively. The chemical analysis, performed on a sample of purified Mt, indicated a highly charged Mt (0.41 eq/formula unit) with a structural formula: $[(Si_{3.89}\ Al_{0.11})\ (Al_{1.43}\ Fe_{0.26}\ Mg_{0.30})]\ M^+_{0.41}$ (Magnoli et al., 2008).

$ODTMA^+$ and $HDTMA^+$ bromides were purchased from Sigma Aldrich Co., purity = 98%, solubility in water, low and 50 mg/mL, respectively, and used as received. The molecular mass of $ODTMA^+$ and $HDTMA^+$ bromides are 392.5 and 364.5 g mol^{-1}, respectively.

2.2. Preparation of organoclays

The synthesis of OMt samples was performed by the following procedure: 20 g of Mt was first dispersed in 1 L of deionized water, to which a desired amount of $ODTMA^+$ or $HDTMA^+$ bromide was slowly added. The concentrations of $ODTMA^+$ and $HDTMA^+$ bromides used were 0.5, 1 and 2 CEC of Mt, respectively. The reaction mixtures were stirred for 5 h at 60 °C. All products were washed by centrifugation to free them of bromide anions (tested by $AgNO_3$), dried at 80 °C and ground in an agate mortar. The OMt samples were labeled, indicating the alkylammonium cations and the concentrations of CEC as: ODTMAX-Mt, HDTMAX-Mt, respectively, with X = 0.5, 1 and 2.

2.3. Material characterization

The total specific surface area (S_t) was determined by water adsorption at room temperature and a relative humidity (RH) of 56% (Laird, 1999; Torres Sánchez and Falasca, 1997) and the external specific surface area (S_{ext}) by nitrogen adsorption at 77 K on samples previously dried at 100 ºC for 6 h at high vacuum, using Micromeritics AccuSorb 2100 E equipment. The internal specific surface area (S_i) was determined as the difference between total (S_t) (Michot and Villieras, 2006; Srodon and Mc Karty, 2008) and external (S_{ext}) specific surfaces.

XRD patterns (reflection (001)) were collected, in the range $3 \leq 2\theta \leq 13^º$, with a counting time of 10 s/step using a Philips 3020 diffractometer operated at 30 mA and 40 kV with Cu$K\alpha$ radiation. The samples were oriented at constant humidity (dispersion samples were dried maintaining a constant RH = 0.47 for 48 h).

Particle size determination was performed on a 10^{-3} M KCl solution with a 1% m/m particle dispersion by dynamic light scattering (DLS) measurements using a Brookhaven 90Plus/Bi-MAS Multi Angle Particle Sizing, operated at: λ = 635 nm, 15 mW solid state laser, scattering angle = 90º, and temperature = 25 ºC. The determination renders the apparent equivalent sphere diameter, D_{app}.

SAXS and WAXS data were obtained at the D01A SAXS line workstation of the Brazilian Synchrotron Light Source (LNLS), Campinas, Brazil, using a wavelength of 0.155 nm and a sample to detector distance of 491.334 mm (details in: http://lnls.cnpem.br/accelerators/accelerator-parameters). The range of q detected allowed spanning $0.25 \leq q \leq 5.9$ nm of range. All measurements were made at room temperature and registered in a 2D-CCD detector (MAR-USA 165 mm). One dimension curves were obtained after integration of 2D data using the program FIT2D (Hammersley et al., 1996). Data were corrected subtracting the parasitic contribution from the total scattering.

The OMt samples' morphology was examined by SEM using a field emission gun scanning electron microscope Zeiss (FEG-SEM Zeiss LEO 982 GEMINI) with combined energy dispersive X-ray spectroscopy (EDS) analyzer, which provided the qualitative and semi-quantitative composition of the samples. Mt and OMt samples were fixed to 10 mm metal mounts using carbon tape, and spit coated with gold under vacuum in an argon atmosphere.

To determine the thermal degradation of Mt and some of the OMt samples, thermogravimetry (TG) tests were performed using a STA 409/c Netzsch instrument. Samples of 50 mg were placed in an aluminum pan and heated from 30 to 1100 ºC, at a scanning rate of 10 ºC/min in Nitrogen atmosphere with a gas flow rate of 40 mL/min.

The electrophoretic mobility was determined in water dispersions of Mt and OMt samples by microelectrophoresis (zeta potential function) in the same Brookhaven equipment utilized for D_{app} measurements, using 10^{-3} M KCl as inert electrolyte and Pd electrodes.

3. Results and discussion

Table 1 shows the specific surface areas: total (S_t), external (S_{ext}), internal (S_i) and apparent particle diameters (D_{app}) of all samples.

Specific surface area values of Mt and HDTMA0.5Mt samples, determined by N_2 adsorption, agree with values obtained by Bojemueller et al. (2001) and Praus et al. (2006), respectively. The decrease of S_{ext} with the alkylammonium salt content was assigned to the diminution of micropore size (Praus et al., 2006) and surfactant occupancy of the interparticle pores, and that of S_t to the stronger interactions produced by the alkylammonium salt layer arrangement in Mt interlayer space (Pospíšil et al., 2002) and external surfaces, and by the formation of rather large aggregates, as indicated by the D_{app} values (Table 1).

Table 1
Total (S_t), external (S_{ext}) and interlayer (S_i) specific surface area and apparent particle diameter (D_{app}) for Mt and OMt samples.

sample	S_t (m^2/g)	S_{ext} (m^2/g)	S_i (m^2/g)	D_{app} (nm)
Mt	621 ± 5.0[a]	34.00 ± 0.16	587	540 ± 28
ODTMA0.5-Mt	74 ± 1.5	4.14 ± 0.14	70	2625 ± 49
ODTMA1-Mt	94 ± 2.2	3.65 ± 0.14	90	3891 ± 63
ODTMA2-Mt	91 ± 0.2	1.83 ± 0.14	89	25276 ± 389
HDTMA0.5-Mt	89 ± 0.7	3.25 ± 0.15	86	3100 ± 59
HDTMA1-Mt	68 ± 0.5	1.86 ± 0.02	66	4233 ± 65
HDTMA2-Mt	19 ± 0.2	2.54 ± 0.20	16	14400 ± 158

[a] Data from Magnoli et al. (2008).

The internal specific surface area (S_i) value of the OMt samples showed a significant drop when compared with Mt, suggesting a high entrance of alkylammonium salts in the interlayer space of the Mt in all the samples.

The OMt's aggregate enlargement with alkylammonium ion loading (Table 1) could be related to micelle formation in the solution and on the OMt samples surfaces. The alkylammoniun concentration values (corresponding to 0.5, 1 and 2 CEC) exceed between 58 and 232 and between 19 and 77 times the critical micelle concentrations (CMC), for $ODTMA^+$ and $HDTMA^+$, respectively (CMC for $ODTMA^+$ and $HDTMA^+$ are 3×10^{-4} and 9×10^{-4} M, respectively; Rosen, 1989). Differences in aggregate sizes found when comparing ODTMAX-Mt samples with HDTMAX-Mt samples could be related to the dissimilar binding coefficients of the monomers adsorbed (Zadaka et al., 2010) and to the higher micelle affinity for the smectite surface (Mishael et al., 2002).

XRD patterns (RH = 0.47) are shown in Fig. 1. Shifts of basal spacing towards higher values with respect to raw Mt position can be observed in all OMt samples. This finding confirmed the entry of alkylammonium ions into the interlayer spaces of the Mt, in agreement with S_i values decrease. OMt samples showed basal spacing ranging from $d_{001} = 1.802$ to 2.160 nm, which are much larger than that of raw Mt ($d_{001} = 1.2581$ nm).

The interlayer space thickness of the OMt samples was determined from their d_{001} values and the Mt layer thickness, 0.97 nm (Emmerich et al., 2001). From XRD, Fig. 1, it was found that HDTMAX-Mt sample interlayer spaces were: 0.83, 1.19 and 1.09 nm for X = 0.5, 1 and 2 CEC loading, respectively. The smaller value found in the 0.5 CEC sample is close to the lateral bilayer height (0.81 nm), while 1.09 and 1.19 nm may be interpreted as pseudotrilayers or paraffin-like monomolecular arrangements (He et al., 2006, and references therein) with tilt angles (α) of 31.95 and 33.43º, respectively, in agreement with data found by He et al. (2006) and Xu and Zhu (2009). For ODTMAX-Mt samples the interlayer spaces found were: 0.95, 1.12, and 1.15 nm for X = 0.5, 1 and 2 CEC loading, respectively. According to Beneke and Lagaly (1987) and Brindley and Moll (1965) models for the arrangement of alkyl chains, which are based upon mutual interlocking, the pseudotrilayer array can explain the basal reflection at 1.92 nm found in ODTMA0.5-Mt. Basal reflection values found at around 2 nm in ODTMA1-Mt and ODTMA2-Mt samples could be explained as due to the pseudotrilayers or paraffin-like monomolecular arrangements with tilt angles of 32.40 and 32.90º, respectively.

A closer view of the ODTMA2-Mt pattern (Fig. 1 inset) indicated the presence of basal spacing values 2.835, 1.408 and 1.065 nm, which could not be assigned to high order lines. They may come, as found by He et al. (2006) in smectite with heavy $HDTMA^+$ loading, from multiphase systems consisting of both regularly and randomly intercalated layers, not detected in HDTMA2-Mt sample XRD pattern. Differences observed in OMt samples loaded with $HDTMA^+$ when comparing present results with He et al. (2006, 2010) and Zhu et al. (2011), can be due to the dissimilarity of the Mt used and to the OMt sample synthesis temperature and, also, to differences in material handling during the synthesis process. The reflection at 2.835 nm could come from a paraffin-type monomolecular arrangement with a tilt angle $\alpha = 42.18$º. The line at 1.408 nm corresponds to an interlayer space of 0.438 nm, a value that agrees with a monolayer arrangement of $ODTMA^+$ with its plane of a zigzag array of the carbon atoms perpendicular to the plane of the Mt layer (He et al., 2006), and the trimethyl head inserted into the hexagonal hole of the basal oxygen plane (Zhu et al., 2003, and references therein) while that at 1.065 nm, could come from partially collapsed layers generated for the removal of inorganic ions and its hydration water in the interlayer space, helped by the surfactant entrance, which provides a hydrophobic environment.

WAXS and SAXS data, from samples kept at RH = 0.47 for 48 h, allowed one to analyze zones not available by XRD (Fig. 2). Examination of I vs q curves showed that both samples with 0.5 CEC loading are monophasic with a basal spacing value compatible with the model of bilayer intercalation of surfactant. Samples with 1 CEC loading and higher presented a well-defined line corresponding to the basal spacing determined through XRD. However, coexistence of different interlayer space values were also observed, confirming XRD observation for HDTMA2-Mt. Samples with 1 CEC loading displayed superposition of broad and poorly defined lines at q values ranging 0.75 to 2.70 nm^{-1} (HDTMA1-Mt) and 0.70 to 2.75 nm^{-1} (ODTMA-1Mt), which corresponded to d_{001} value ranges: 3.80 to 4.20 nm and 5.60 to 6.10 nm, respectively. They could be assigned to perpendicular interlocked, or paraffin-like type models with tilting angles $\alpha = 35$º and/or 60º. A weaker signal at 4.43 nm^{-1} (HDTMA1-Mt) and 4.23 nm^{-1} (ODTMA1-Mt) indicative of interlayer space values of 1.45 and 1.50 nm, respectively, could also be distinguished. Latter values have not been observed in WAXS data (deposited as supplementary material) obtained from samples kept at ambient conditions before SAXS experiments. The HDTMA2-Mt sample presented a SAXS and WAXS I vs q curve resembling those of 1 CEC samples but with different relative intensities, while in the ODTMA2-Mt curve well defined lines could be detected and were assigned to interlayer space values of 1.39, 2.06, 2.83 and 4.13 nm. The origin of the first three interlayer space values have been described above, and the last one could be assigned to a paraffin-type bilayer arrangement with $\alpha = 48$º.

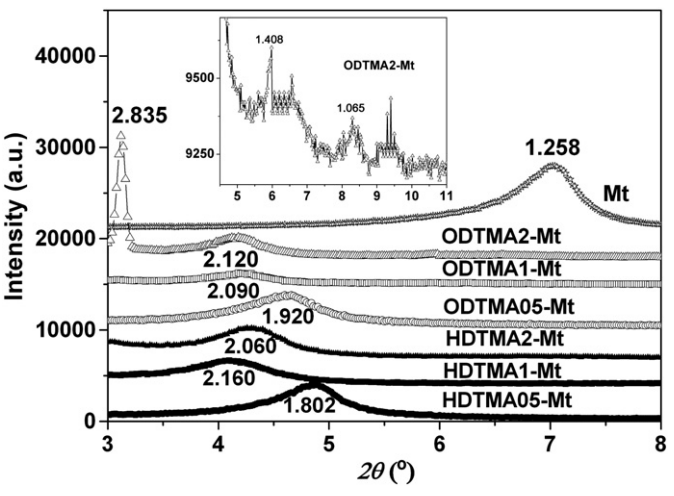

Fig. 1. XRD patterns, basal plane distances in nm, uncertainties are 1×10^{-3} nm.

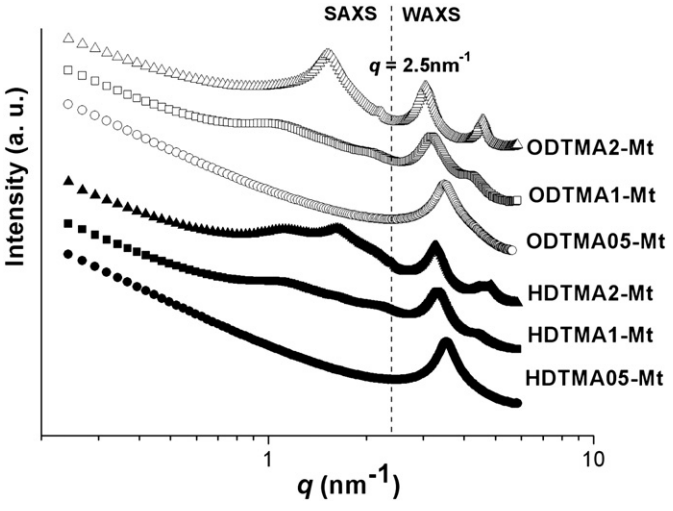

Fig. 2. Log-log SAXS curves for all prepared OMt samples kept at RH = 0.47 for 48 h.

It could be seen from XRD and WAXS data (Figs. 1 and 2, respectively), that in all the organo-montmorillonites part of the organic cations were included like monolayers with their chains laying parallel to the Mt layers ($1.39 \leq d_{001} \leq 1.45$ nm) (Brindley and Moll, 1965). It was also found that all the OMt samples showed more intense lines at $1.90 \leq d_{001} \leq 2.15$ nm, which were compatible with a pseudo trilayer (Zhu et al., 2003) or a disordered liquid-like monolayer (Pospíšil et al., 2002).

SAXS data analysis evidenced that the 2 CEC loading of both alkylammonium cations induce further lines ($3.90 \leq d_{001} \leq 4.15$ nm), in accordance with paraffin-like bilayers with a tilt angle in the range 35° to 48º. A broader and less intense line could be seen in samples with 2 CEC $HDTMA^+$ loading and 1 CEC of both alkylammonium loading (ranging: $5.60 \leq d_{001} \leq 5.90$ nm), which is consistent with paraffin-like bilayers with a tilt angle of approximately 60° (Zhu et al., 2003). In paraffin-like bilayers, alkyl chain interactions would be stronger helping an ordered chain packing with smaller chain–silicate surface interaction, suitable for polymers entrance.

Results presented here indicate levels of surfactant loading values required to reach some levels of basal spacings different from those determined by He et al. (2010). This may be due to the Patagonian Mt CEC value which is 70% higher than the highest CEC value of the smectites employed by the mentioned authors. In accordance with He et al. findings (2010) basal spacing modifications have also been found in OMt with 1 CEC loading and higher, when comparing data from samples stored at ambient conditions with those maintained in a humidity controlled environment (RH = 0.47) for 48 h. Raw Mt also showed coexistence of diverse basal spacing values due to environmental differences (see Fig. 1S). He et al. (2010) interpreted environmental effects (aging, drying, rehydrating) on OMt samples as coming from heterogeneities in their interlayer structure. The observations in this work differ also from the stepwise increase in basal spacing with surfactant loading found by other authors (De Paiva et al., 2008; Lee et al., 2005).

A SEM image of Mt (Fig. 3A) showed curved plates either with face-to-edge contacts between particles or covered by small and well-separated particles. Random orientation and a uniform size of around 1 μm, could be estimated. SEM micrographs of OMt samples (Fig. 3B, C, D and E) indicated morphology modifications of the Mt surface structure induced by diversity in alkylammonium salt intercalation. Sample HDTMA1-Mt showed no significant morphological changes with respect to Mt; only a higher agglomeration could be identified, which was consistent with the increase of the D_{app} value

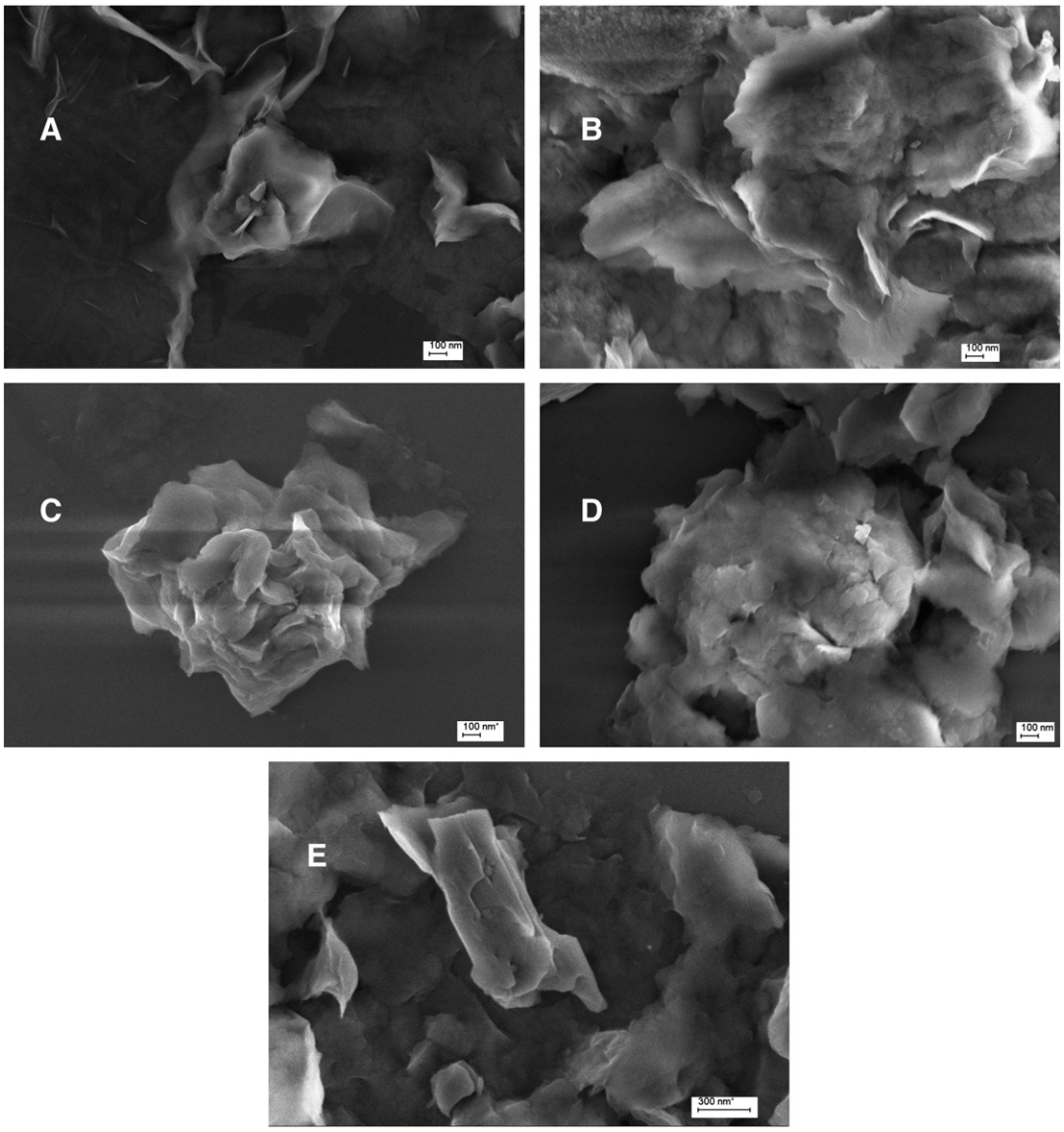

Fig. 3. SEM micrographs of (A) Mt; (B) HDTMA1-Mt and (C) HDTMA2-Mt; (D) ODTMA1-Mt and (E) ODTMA2-Mt samples.

(Table 1). HDTMA2-Mt and ODTMA1-Mt sample particles exhibited less curved plates and aggregate formation, similar to those observed by He et al. (2006). Lee et al. (2005) using TEM and XRD data compared the interlayer structure of two different Mt intercalated with $HDTMA^+$. They found that the amount of $HDTMA^+$ adsorbed on each sample varies related to the CEC and surface charge density values. Different from Lee et al. (2005) and He et al. (2006), current results show that at the same 2 CEC loading only the more regular intercalation, seen in ODTMA2-Mt from SAXS data, was reflected in the occurrence of flat plates, as could be observed in the SEM micrograph, shown in Fig. 3E. Comparison of our results with those of He et al. (2010) seems to indicate that the longer alkylammonium chain helps to reach an ordered intercalation and flat plates at 2 CEC loading, while in spite of the rather small chain difference, 2 CEC loading of $HTDMA^+$ is not enough to obtain a similar microstructure.

Effective surfactant loading of some of the OMt samples was further examined from their mass loss between 200 and 550 ºC. Mt sample was also analyzed for comparison reasons. The surfactants decompose within the mentioned temperature range (Xie et al., 2002). The percentage of mass loss found (46.1 (ODTMA2-Mt); 32.4 (ODTMA1-Mt); 31.6 (HDTMA2-Mt); 26.5 (HDTMA1-Mt) and 4.05% (Mt)) was coherent with the loaded amount of surfactants.

Differences observed between the results presented here and those found by other authors may be assigned to the charge density of the Mt sample (0.41 eq/formula unit), higher than that utilized by He et al. (2006) (0.33 eq/formula unit) and by Lee et al. (2005) (0.31 and 0.35 eq/formula unit). This would affect the arrangement of adsorbed surfactant layers (Lagaly, 1994; Lee et al., 2005, and references therein). The structure of grain-type and agglomerates found in the present OMt samples can be assigned to the ability of the particles to form aggregates, which is greater than that of raw Mt, according with D_{app} values, Table 1. This feature is due to the surfactants that compensate the negative charge of the particles and, thus, eliminate the repulsive electrostatic forces between them (Pospíšil et al., 2001).

Fig. 4 shows the zeta potential vs *pH* curves for all the studied samples. The Mt zeta potential depicted a flat curve (around −30 mV), without significant change over a wide *pH* range (from pH 2 to 8), similar to that published in the literature (Durán et al., 2000; Lombardi et al., 2006; Sondi et al., 1996; Thomas et al., 1999). This pH-independent zeta potential behavior of Mt was originated in the constant surface potential (structure or basal sites) and variable charge (edge sites) of Mt. At a critical value of the potential, adjustments between the Stern layer and the diffuse layer kept the potential constant (Miller and Low, 1990).

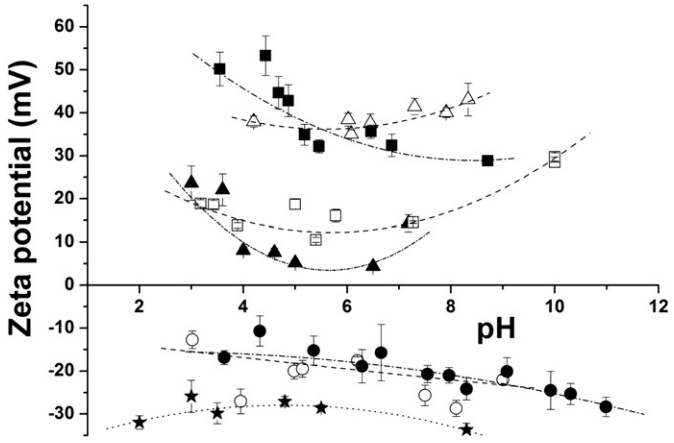

Fig. 4. Zeta potential vs pH curves of all samples. Symbols indicate: (⋆) Mt; (●) 0.5; (■) 1 and (▲) 2 CEC loadings. Solid symbols for $HDTMA^+$ and open for $ODTMA^+$ loaded Mt samples.

Heath and Tadros (1983) and more recently Durán et al. (2000) agreed to define an IEP_{edge} for Mt at a pH value of approximately 7, and due to the small surface area of edges (around 1–3% of the total specific surface area S_t), they indicated that these sites can only cause small pH dependence. On the contrary, Thomas et al. (1999) pointed out that the measured Mt zeta potential corresponded to the amphoteric sites of the edge surface, which were negatively charged at pH values above 3 and, then, they calculated IEP_{edge} at a pH around 3.6. This value agreed well with the IEP at pH = 2.7 determined in our Mt sample (Magnoli et al., 2008) by a diffusion potential method (Tschapek et al., 1989).

Churchman (2002) informed an Mt charge reversal, by adsorption of quaternary ammonium derivatives of polymers, from a net negative charge at zero loading to a net positive charge as the polycation content increased. This behavior was explained by the entrance of polycations into the Mt interlayer space and simultaneously, even at very low loadings (i.e. at 0.5 CEC), by a significant adsorption of polycations on the external surfaces. Radian and Mishael (2008) have also found that a low loading of quaternary ammonium polycations was required to neutralize and reverse the Mt charge surface. Those results could only be explained by the screening of the Mt surface even at loadings lower than stoichiometric neutralization.

In the present samples no charge reversal was attained for 0.5 loading of both alkylammonium salts employed, though modification of zeta potential values was evident (ranging from −20 to −15 mV). Larger loadings (1 CEC and higher) of both alkylammonium reversed the surface charge of Mt as could be seen in Fig. 4 zeta potential curves. Results presented here indicated that the edge and external surface were progressively covered by alkylammonium groups in bilayer arrangements (Praus et al., 2006) with some positive ammonium groups oriented out of the surface.

Zadaka et al. (2010) reported a linear correlation between zeta potential and the adsorption of organic cations up to the CEC value, while a non-linear increase in zeta potential was found for cation adsorption exceeding the Mt CEC. Later behavior was assigned to polymer extension into the solution, surface screening, micelle formation and affinity of the cations for the Mt (Mishael et al., 2002; Rytwo et al., 1996).

Current OMt samples show two different behaviors when comparing the zeta potential curves of both alkylammonium cations adsorbed on the Mt (Fig. 4). For ODTMAX samples a continuous increase of zeta potential values with surfactant loading was found. For HDTMAX samples with up to 1 CEC loading a behavior similar to that of ODTMAX samples was also observed, as expected. However, a further increase of $HDTMA^+$ loading reduced the zeta potential value keeping it positive.

A lower amount of alkylammonium in the external surface of HDTMA2-Mt when compared with that ODTMA2-Mt may explain the decrease of zeta potential value when going from 1 to 2 CEC loading of $HDTMA^+$. This assumption is in agreement with the observed lower D_{app} value in HDTMA2-Mt, Table 1, and with the morphological differences observed when comparing SEM micrographs of both samples, Fig. 3.

4. Conclusions

Organo-montmorillonites have been prepared using Patagonian Mt at three distinct loadings (0.5, 1 and 2 CEC) of two trialkylammonium salts of different alkyl chain length ($ODTMA^+$ and $HDTMA^+$). Both surfactants induce swelling at all loadings; 0.5 CEC loadings generate monophasic OMt samples with similar properties regarding basal spacing, total surface, internal surface, aggregate formation, surface charge and no influence of ambient conditions. Higher loadings yield OMt samples with different characteristics: 1 and 2 CEC loading of $HDTMA^+$ and 1 CEC of $ODTMA^+$ samples present a distribution of interlayer space values covering a wide range. While the 2 CEC $ODTMA^+$ sample shows several but well-defined interlayer space values, denoting a

structural regularity that is reflected in its flat plate particles. At all loadings both surfactants occupy not only Mt interlayer spaces but also particle surfaces, inducing surface charge modification and reversal in samples produced with 1 or higher CEC loadings.

The organization of alkylammonium cations in paraffin-type bilayer arrangements within the interlayer spaces in OMt samples loaded with 1 CEC or higher would help polymer entrance for CPN applications.

Supplementary data to this article can be found online at http://dx.doi.org/10.1016/j.clay.2013.08.032.

Acknowledgments

The authors acknowledge financial help from Ministerio de Ciencia y Técnica, Agencia Nacional de Promoción Científica y Tecnológica, MINCyT-ANPCyT-FONCyT through PICT 1360, PICT06 2315 and through FONARSEC FSNano-008, Consejo Nacional de Investigaciones Científicas y Técnicas (CONICET), PIP 0985 and Universidad Nacional de La Plata (Project X-577), Argentina; Laboratório Nacional de Luz Síncrotron (LNLS), Brazil, and Consejo Superior de Investigación Científica (CSIC), Spain. G.P. and R.M.T.S. are members of CONICET, and M.F. and M.P. acknowledge a CONICET fellowship.

References

Alexandre, M., Dubois, P., 2000. Polymer-layered silicate nanocomposites: preparation, properties and uses of a new class of materials. Mater. Sci. Eng. R. 28, 1–63.
Beneke, K., Lagaly, G., 1987. Layered chlorotin arsenate and chlorotin phosphate. Inorg. Chem. 26, 2537–2542.
Benetti, E.M., Causin, V., Marega, C., Marigo, A., Ferrara, G., Ferraro, A., Consalvi, M., Fantinel, F., 2005. Morphological and structural characterization of polypropylene based nanocomposites. Polymer 46, 8275–8285.
Bojemueller, E., Nennemann, A., Lagaly, G., 2001. Enhanced pesticide adsorption by thermally modified bentonites. Appl. Clay Sci. 18, 277–284.
Botana, A., Mollo, M., Eisenberg, P., Torres Sánchez, R.M., 2010. Effect of modified montmorillonite on biodegradable PHB nanocomposites. Appl. Clay Sci. 47, 263–270.
Brindley, G.W., Moll, W.F., 1965. Complexes of natural and synthetic Ca montmorillonites with fatty acids. Am. Mineral. 50, 1355–1370.
Churchman, G.J., 2002. Formation of complexes between bentonite and different cationic polyelectrolytes and their use as sorbents for non-ionic and anionic pollutants. Appl. Clay Sci. 21, 177–189.
De Paiva, L.B., Morales, R.M., Valenzuela Diaz, F.R., 2008. Organoclays: properties, preparation and applications. Appl. Clay Sci. 42, 8–24.
Durán, J.D.G., Ramos-Tejada, M.M., Arroyo, F.J., González-Caballero, F., 2000. Rheological and electrokinetic properties of Na-montmorillonite suspensions. J. Colloid Interface Sci. 229, 107–117.
Emmerich, K., Plötze, M., Kahr, G., 2001. Reversible collapse and Mg^{2+} release of de- and re-hydroxylated homoionic cis-vacant montmorillonites. Appl. Clay Sci. 19, 143–154.
Fox, J.B., Ambuken, P.V., Stretz, H.A., Peascoe, R.A., Payzant, E.A., 2010. Organo-montmorillonite barrier layers formed by combustion: Nanostructure and permeability. Appl. Clay Sci. 49, 213–223.
Hammersley, A.P., Svensson, S.O., Hanfland, M., Fitch, A.N., Hdusermann, D., 1996. Two-dimensional detector software: from real detector to idealised image or two-theta scan. High Press. Res. 14, 235–248.
He, H., Frost, R.L., Bostrom, T., Yuan, P., Duong, L., Yang, D., Xi, Y., Kloprogge, J.T., 2006. Changes in the morphology of organoclays with $HDTMA^+$ surfactant loading. Appl. Clay Sci. 31, 262–271.
He, H., Ma, Y., Zhu, J., Yuan, P., Qing, J., 2010. Organoclays prepared from montmorillonites with different cation exchange capacity and surfactant configuration. Appl. Clay Sci. 48, 67–72.
Heath, D., Tadros, Th.F., 1983. Influence of pH, electrolyte, and poly(vinyl alcohol) addition on the rheological characteristics of aqueous dispersions of sodium montmorillonite. J. Colloid Interface Sci. 93, 307–319.
Hendricks, S., Teller, E., 1942. X-ray interference in partially ordered layer lattices. J. Chem. Phys. 10, 147–167.
Isitman, N.A., Kaynak, C., 2011. Nanostructure of montmorillonite barrier layers: a new insight into the mechanism of flammability reduction in polymer nanocomposites. Polym. Degrad. Stab. 96, 2284–2289.
Kojima, Y., Usuki, A., Kawasumi, M., Okada, A., Fukushima, Y., Kurauchi, T., Kamigaito, O., 1993. Mechanical properties of nylon 6-clay hybrid. Mater. Res. Soc. 8 (5), 1185–1189.
Kornmann, X., Lindburg, H., Berglund, L.A., 2001. Synthesis of epoxy–clay nanocomposites. Influence of the nature of the curing agent on structure. Polymer 42, 4493–4499.
Lagaly, G., 1986. Interaction of alkylammines with different types of layered compounds. Solid State Ionics 22, 43–51.
Lagaly, G., 1994. Layer charge determination by alkylammonium ions. In: Mermut, A. (Ed.), Charge Characteristics of 2:1 Clay Minerals. CMS Workshop Lectures, 6. The Clay Minerals Society, Boulder, CO, pp. 1–46.
Lagaly, G., Barrer, R.M., Goulding, K., 1984. Clay–organic interactions and discussion. Philos. Trans. R. Soc. Lond. A 14 (311), 315–332.
Laird, D.A., 1999. Layer charge influences on the hydration of expandable 2:1 phyllosilicates. Clay Clay Miner. 47, 630–636.
Lee, S.Y., Cho, W.Y., Hahn, P.S., Lee, M., Lee, Y., Kim, K.J., 2005. Microstructural changes of reference montmorillonites by cationic surfactants. Appl. Clay Sci. 30, 174–180.
Li, Y., Ishida, H., 2003. Concentration-dependent conformation of alkyl tail in the nanoconfined space: hexadecylamine in the silicate galleries. Langmuir 19, 2479–2484.
Lin, J.J., Chen, I.J., Chou, C.C., 2003. Critical conformational change of poly(oxypropylene) diamines in layered aluminosilicate confinement. Macromol. Rapid Commun. 24, 492–503.
Lombardi, B., Torres Sánchez, R.M., Eloy, P., Genet, M., 2006. Interaction of thiabendazole and benzimidazole with montmorillonite. Appl. Clay Sci. 33, 59–65.
Magnoli, A.P., Tallone, L., Rosa, C., Dalcero, A.M., Chiacchiera, S.M., Torres Sánchez, R.M., 2008. Commercial bentonites as detoxifier of broiler feed contaminated with aflatoxin. Appl. Clay Sci. 40, 63–71.
Michot, L.J., Villieras, F., 2006. Surface area and porosity. In: Bergaya, F., Theng, B.K., Lagaly, G. (Eds.), Handbook of Clay Sci. Developments in Clay Sci., 1. Elsevier, Amsterdam, pp. 965–978.
Miller, S.E., Low, P.F., 1990. Characterization of the electrical double layer of montmorillonite. Langmuir 6, 572–578.
Mishael, Y.G., Undabeytia, T., Rytwo, G., Papahadjopoulos-Sternberg, B., Rubin, B., Nir, S., 2002. Sulfometuron incorporation in cationic micelles adsorbed on montmorillonite. J. Agric. Food Chem. 50, 2856–2863.
Pospíšil, M., Capková, P., Merínská, D., Malác, Z., Šimoník, J., 2001. Structure analysis of montmorillonite intercalated with cetylpyridinium and cetyltrimethylammonium: molecular simulations and XRD analysis. J. Colloid Interface Sci. 236, 127–131.
Pospíšil, M., Capková, P., Merínská, D., Malác, Z., Šimoník, J., 2002. Intercalation of octadecylamine into montmorillonite: molecular simulations and XRD analysis. J. Colloid Interface Sci. 245, 126–132.
Pospíšil, M., Kalendová, A., Capková, P., Šimoník, J., Valášková, M., 2004. Structure analysis of intercalated layer silicates: combination of molecular simulations and experiment. J. Coll. Interf. Sci. 277, 154–161.
Praus, P., Turicová, M., Študentová, S., Ritz, M., 2006. Study of cetyltrimethylammonium and cetylpyridinium adsorption on montmorillonite. J. Colloid Interface Sci. 304, 29–36.
Radian, A., Mishael, Y., 2008. Characterizing and designing polycation-clay nanocomposites as a basis for imazapyr controlled release formulations. Environ. Sci. Technol. 42, 1511–1516.
Rosen, M.J., 1989. Surfactants and Interfacial Phenom, 2nd ed. Wiley & sons, N. York.
Rytwo, G., Nir, S., Margulies, L., 1996. A model for adsorption of divalent organic cations to montmorillonite. J. Colloid Interface Sci. 181, 551–560.
Sondi, I., Bišćan, J., Pravdić, V., 1996. Electrokinetics of pure clay minerals revisited. J. Colloid Interface Sci. 178, 514–522.
Srodon, J., Mc Karty, D.K., 2008. Surface area and layer charge of smectites from CEC and EGME/H_2O retention measurements. Clay Clay Miner. 56, 155–174.
Thomas, F., Michot, L.J., Vantelon, D., Montarges, E., Prelot, B., Cruchaudet, M.J., Delon, F., 1999. Layer charge and electrophoretic mobility of smectites. Colloids Surf. A 159, 351–358.
Tiwari, R.R., Khilar, K.C., Natarajan, U., 2008. Synthesis and characterization of novel organo-montmorillonites. Appl. Clay Sci. 38, 203–208.
Torres Sánchez, R.M., Falasca, S., 1997. Specific surface and surface charges of some Argentinian soils. Z. Pflanzenernaehr. Bodenkd. 160, 223–226.
Tschapek, M., Torres Sánchez, R.M., Wasowski, C., 1989. Handy methods for determining the isoelectric point of soils. Z. Pflanzenernaehr. Bodenkd. 152, 73–76.
Vaia, R.A., Wagner, H.D., 2004. Framework for nanocomposites. Mater. Today 7, 32–37.
Weon, J.-I., Sue, H.-J., 2005. Effects of clay orientation and aspect ratio on mechanical behaviour of nylon-6 nanocomposite. Polymer 46, 6325–6334.
Williams-Daryn, S., Thomas, R.K., 2002. The intercalation of a vermiculite by cationic surfactants and its subsequent swelling with organic solvents. J. Colloid Interface Sci. 255, 303–311.
Xie, W., Xie, R., Pan, W.P., Hunter, D., Koene, B., Tan, L.S., Vaia, R., 2002. Thermal stability of quaternary phosphonium modified montmorillonites. Chem. Mater. 14 (11), 4837–4845.
Xu, L., Zhu, L., 2009. Structures of OTMA- and DODMA-bentonite and their sorption characteristics towards organic compounds. J. Colloid Interface Sci. 331, 8–14.
Zadaka, D., Radian, A., Mishael, Y.G., 2010. Applying zeta potential measurements to characterize the adsorption on montmorillonite of inorganic, cations as monomers, micelles or polymers. J. Colloid Interface Sci. 352, 171–177.
Zhao, Z., Tang, T., Qin, Y., Huang, B., 2003. Relationship between the continually expanded interlayer distance of layered silicates and excess intercalation of cationic surfactants. Langmuir 19, 9260–9265.
Zhu, J., He, H., Guo, J., Yang, D., Xie, X., 2003. Arrangement models of alkylammonium cations in the interlayer of $HDTMA^+$ pillared montmorillonites. Chin. Sci. Bull. 48 (368), 372.
Zhu, J., Wang, T., Zhu, R., Ge, F., Yuan, P., He, H., 2011. Expansion characteristics of organo montmorillonites during the intercalation, aging, drying and rehydration processes: effect of surfactant/CEC ratio. Colloids Surf. A 384, 401–404.